Costa, A. M., Freitas, M. da C., Leira, M., Costas, S., Costa, P. J., Andrade, C., Bao, R., Duarte, J., Rodrigues, A., Cachão, M., Araújo, A. C., Diniz, M., & Arias, P. (2019). The role of climate, marine influence and sedimentation rates in late-Holocene estuarine evolution (SW Portugal). *The Holocene*, *29*(4), 622-632.
https://doi.org/10.1177/0959683618824768

The role of climate, marine influence and sedimentation rates in Late Holocene estuarine evolution (SW Portugal)

Ana M. Costa[a,b,c,*], M. Conceição Freitas[c,d], Manel Leira[c,f], Susana Costas[e], Pedro J. M. Costa[c,d], César Andrade[c,d], Roberto Bao[f], João Duarte[g], Aurora Rodrigues[g], Mário Cachão[c], Ana Cristina Araújo[a,h], Mariana Diniz[h], Pablo Arias[b]

a – LARC – DGPC and CIBIO / InBIO, Rua da Bica do Marquês 2, 1300-087 Lisboa, Portugal
b – IIIPC (Universidade de Cantábria, Gobierno de Cantabria), Avda de los Castros 52, 39005 Santander, Spain
c – Instituto Dom Luiz (IDL), Faculdade de Ciências, Universidade de Lisboa, Edifício C6, Piso 3, Campo Grande, 1749-016 Lisboa, Portugal
d - Departamento de Geologia, Faculdade de Ciências, Universidade de Lisboa, Edifício C6, Piso 3, Campo Grande, 1749-016 Lisboa, Portugal
e – CIMA, Universidade do Algarve, Campus de Gambelas, Ed.7, 8005-139 Faro, Portugal
f – Centro de Investigacións Científicas Avanzadas (CICA), Facultade de Ciencias, Universidade da Coruña, 15071 A Coruña, Spain
g – Instituto Hidrográfico, Rua das Trinas 49, 1296-093 Lisboa, Portugal
h – UNIARQ, Universidade de Lisboa, Alameda da Universidade, 1600-214 Lisboa, Portugal

* - corresponding author: Ana Maria Costa, institution: LARC/DGPC and EnvArch / CIBIO / InBIO, address: Rua da Bica do Marquês 2, 1300-087 Lisboa, mail: acosta@dgpc.pt, phone number: +351213627356

M. Conceição Freitas - cfreitas@fc.ul.pt; Manel Leira - mlcampos@fc.ul.pt; Susana Costas - scotero@ualg.pt; Pedro J.M. Costa – ppcosta@fc.ul.pt; César Andrade - candrade@fc.ul.pt; Roberto Bao - roberto.bao@udc.es; Aurora Rodrigues - aurora.bizarro@hidrografico.pt; João Duarte - joao.duarte@hidrografico.pt; Mário Cachão - mcachao@fc.ul.pt; Ana Cristina Araújo - acaraujo@dgpc.pt; Mariana Diniz - m.diniz@letras.ulisboa.pt; Pablo Arias - pablo.arias@unican.es

Abstract

Estuaries are sensitive to changes in global to regional sea level to climate-driven variation in rainfall and to fluvial discharge. In this study, we use source and environmentally sensitive proxies together with radiocarbon dating to examine a 7 m-thick sedimentary record from the Sado estuary accumulated throughout the last 3.6 kyr. The lithofacies, geochemistry and diatom assemblages in the sediments accumulated between 3570 and 3240 cal. BP indicate a mixture between terrestrial and marine sources. The relative contribution of each source varied through time as sedimentation progressed in a low intertidal to high subtidal and low-energy accreting tidal flat. The sedimentation proceeded under a general pattern of drier and higher aridity conditions, punctuated by century-long changes of the rainfall regime that mirror an increase in storminess that affected SW Portugal and Europe. The sediment sequence contains evidence of two periods characterized by downstream displacement of the estuarine/freshwater transitional boundary, dated to 3570-3400 cal. BP and

3300-3240 cal. BP. These are intercalated by one episode where marine influence shifted upstream. All sedimentation episodes developed under high terrestrial sediment delivery to this transitional region, leading to exceptionally high sedimentation rates, independently of the relative expression of terrestrial/marine influences in sediment facies. Our data show that these disturbances are mainly climate-driven and related to variations in rainfall and only secondarily with regional sea-level oscillations. From 3240 cal. BP onwards, an abrupt change in sediment facies is noted, in which the silting estuarine bottom reaches mean sea level and continued accreting until present under prevailing freshwater conditions, the tidal flat changing to an alluvial plain. The environmental modification is accompanied by a pronounced change in sedimentation rate that decreased by two orders of magnitude, reflecting the loss of accommodation space rather than the influence of climate or regional sea-level drivers.

Keywords

Fluvial discharge, Climate variability, Storminess, Sea-level oscillation, Environmental proxies

1. Introduction

Estuaries are transitional areas between fluvial and marine environments. They are also sheltered areas and, rich in natural resources, thus attractive for human settlement and development of human activities since Pre-history. The estuarine basin is a sediment sink for a mixture of materials transported downstream by the hydrographic network and moving landwards from the sea (Schubel, 1982) frequently presenting high sedimentation rates and often offering conditions for high resolution environmental studies (e.g., Colman et al., 2002). As transitional environments, they are actively controlled by river discharge, flooding and sediment availability (e.g., Brown, 1997) and are very sensitive to global and regional sea-level oscillations (e.g., Wong et al., 2014; Little et al., 2017).

In the recent past, changes in river discharge and terrestrial sediment inputs of both solid and dissolved loads have been extensively modified and controlled by dam construction (e.g., Azevêdo et al., 2010). In a more distant past, anthropic disturbances on landscape are documented since the Middle Holocene (e.g., Carrión et al., 2010 and references therein) promoting soil erosion and sediment availability , eventually discharged in estuaries. However, natural changes in freshwater discharge, transport of particulate and dissolved materials delivered to estuaries, as well as changes in estuarine circulation, stratification and residence time have been primarily driven by climate-related conditioning (e.g. drought frequency and duration; e.g., Azevêdo et al., 2010; Shaha and Cho, 2016).

Liu et al. (2007) showed that freshwater discharge is the dominant factor controlling the extent of saline intrusion in the Danshuei estuary (Taiwan), and Azevêdo et al. (2010) concluded that stable river flows are more effective than highly variable flow regimes in controlling estuarine stability in terms of salinity and dispersion of contaminants. Nowadays, despite anthropic factors (e.g., dam, land-use) controlling river flows, trends in freshwater discharges to a large extent still retain the signal of regional changes in precipitation and temperature (e.g., Jiménez Cisneros et al., 2014). In the case of south Europe, river flows have decreased in the last 60 years (e.g., Jiménez Cisneros et al., 2014; Kovats et al., 2014). Due to the lack of long records, the trends in river flows cannot be attributed with confidence to climate changes. However the decrease in river discharges in south Europe appears to accompany the trend in warming and drying climate and to more intense and long meteorological droughts (e.g., Sousa et al., 2011; Jiménez Cisneros et al., 2014; Kovats et al., 2014).

Regional sea-level oscillations are of extreme importance since they frequently deviate from the global mean values and can substantially affect coastal areas (e.g., Church et al., 2013; Wong et al., 2014). A number of sea-level curves have been published for the central Portuguese coast (e.g., Vis et al., 2008; Leorri et al., 2012; Costas et al., 2016a; García-Artola et al., 2018) and they consistently point to a period of rapid sea-level rise since the Last Glacial Maximum until ca.7000 cal. BP. This was followed by a significant attenuation of the rate of sea-level rise until present. A relatively constant sea-level rise rate of 0.31±0.02 mm yr^{-1} throughout the Late Holocene was suggested by Costas et al. (2016a) for the Southwestern Portuguese coast, despite small and short-term departures from the overall average, which were tentatively related to climate variability.

The objective of present study is to investigate the evolution of the fluvial-estuarine boundary of the Sado estuary during the Late Holocene relating spatial shifts of that interface with oscillations of the regional sea-level and climate-driven changes of riverine flow. This work contributes to the broader goal of characterizing the environment and the landscape changes occurred during the Early-Middle Holocene transition and the early phase of the Middle Holocene, when Mesolithic communities (ca. 8400-7000 cal. BP; e.g., Peyroteo-Sternja, 2016) lived and exploited the Sado estuary surroundings (Fig.1).

We analysed several environmental-sensitive proxies in a ca.7m-long sediment core – Arapouco – collected from one of the fluvial systems of SW Portugal - the Sado River (Fig. 1). The proxies indicate a higher marine influence throughout the Late Holocene in an area that is, at present, dominated by fluvial sedimentation. This contrast raises the question: is this marine influence printed in the sediment as a response to an impulse in transgression rate or was it due to a period of reduced river flow?

Answers to this question can be of great importance in the present-day and forthcoming scenarios of global sea-level rise and (extreme) drought conditions that have prevailed in the recent past in southern Portugal (e.g., Costa and Soares, 2009; Santos et al., 2010).

Figure 1 - Location of the Arapouco sediment core (black star).

2. Regional Setting

The Sado estuary is located on the western Portuguese coast (Fig. 1). The Sado river has a maximum length of ca.175km and drains a ca.7700km^2 sizeable watershed (INE, 2007). It runs northward until the confluence with Ribeira de Odivelas (Fig.1) where it bends to the northwest until its mouth, near the city of Setúbal (Fig.1). The terminal area corresponds to a bar-built estuary occupying about ca.140km^2 (Bettencourt et al., 2003) protected by the Tróia sand spit. The estuary extends for a maximum length of 70km reflecting the maximum marine intrusion (herein considered as the fluvial-estuarine boundary) or 77km if the upper limit of tidal rise and fall is considered (Bettencourt et al., 2003).

Ground Penetrating Radar and OSL dating at Tróia spit documented the growth history of the Peninsula in the last 6500 years (Costas et al., 2015). The northwards elongation of the Tróia spit from this date onwards reduced water exchange between the sea and the river and promoted the onset of low energy conditions allowing sediment deposition within the estuary (Costas et al., 2015) and favouring the aggradation of the alluvial plain. The estuary has a Mediterranean flow regime with discharge of ca.1m^3 s^{-1} during the dry season and 50 to 80m^3 s^{-1} during the rainy season that occasionally reaches 470m^3 s^{-1} (Bettencourt et al., 2003 and references therein), causing the flooding of alluvial plains along the margins of the main channel. Estuarine tides are semi-diurnal, the tidal range varying between 1.5 at Neap tides and 3.9m at Spring tides (Bettencourt et al., 2003).

The Sado River cuts across and collects sediment from Caenozoic and Palaeozoic rocks. In its initial course it crosses Palaeozoic turbidites (shales and greywakes), and also volcanic rocks bearing massive sulfide pollymetalic deposits of the Iberian Pyrite Belt (Pimentel et al., 2001; Matos and Oliveira, 2003). In the study area (Arapouco, located upstream Alcácer do Sal, Fig. 1), the river channel runs through Caenozoic sediments mainly constituted of conglomerates, sands and pelites from “Vale do Guizo” and “Marateca” Formations (Antunes et al., 1991; Gonçalves and Antunes, 1992), despite some limestone outcropping at the top of the Vale do Guizo formation. In the left margin of the Sado, near Arapouco, the “Alcácer do Sal” formation (Antunes et al., 1991; Gonçalves and Antunes, 1992), comprising essentially conglomerates, biocalcarenites and sandstones, outcrops. Aeolian quartz-rich sands dated from Plistocene/Holocene extend over the study area (Gonçalves and Antunes, 1992). Near Arapouco and along the right margin, just before the confluence with Ribeira de Sta. Catarina, slaty pelitic rocks, siltites and greywakes of the "Mértola Formation" outcrop reaching a height of 132m at the Sra. da Conceição vertex point (Antunes et al., 1991). At the left margin, the Caenozoic sediments also form a steep slope achieving heights ca.50m. Most of the Mesolithic shell middens identified on the Sado surroundings occur at 40-50m altitude, on the top of the Caenozoic slopes, reaching ca.20km river upstream as far as Herdade de Arapouco to Quinta de D. Rodrigo (e.g., Diniz and Arias, 2012; Fig. 1).

In the study area, the fluvial channel feeds an alluvial plain ranging between 50 and 100m in width. The channel with a mean depth of 1m (Bettencourt et al., 2003; Brito, 2009) is incised in alluvial sediments that reach ca.2m (Table 1) above mean sea level (*msl*). The alluvial plain of Sado river is intensely used for rice production among other agricultural practices since at least the 18th century.

3. Material and methods

3.1 Sediment sampling

Two partially overlapping sediment cores (Arapouco2 and Arapouco 3, located a few meters apart) were collected at Herdade de Arapouco (Fig.1) on the Sado alluvial plain adjacent to the left margin of the channel, close to the present-day fluvial-estuarine boundary within the inner estuary. Both sections (Arapouco2, extending from surface at 2.2m msl to -0.48m msl; and Arapouco3, extending from 0.2m msl to -4.7m msl) were collected using Van der Horst and Livingstone core samplers and overlap for 68cm (Table 1). The two sections were later combined to yield a composite core (hereafter designated Arapouco) with a total length of 690cm. At the base of the core the sediment became coarser and little material was recovered between ca.645cm and 690cm. Topographic data (coordinates and altimetry) were collected using a Global Navigation Sattelite Systems (GNSS) roving receiver units (Leica Geosystems models GPS 900 and NetRover) that operated in real-time, connected to Portuguese internet-based correction services.

Table 1 – Location and altimetry of the analysed sediment cores Arapouco2 and Arapuco3. Coordinates are provided in ERTS89 TM06 Portugal coordinate system. Elevations are given relatively to mean sea level (*msl*).

One surface sediment sample (composed mostly of mud) was collected from the margin of the Sado main channel at Arapouco, to characterize the organic material accumulating at present in this area.

3.2 Sediment analysis

Arapouco core was opened, described and sub-sampled every 2cm in the laboratory. Sediment sub-samples were subsequently freeze-dried, split and a representative quantity was ground using a Retsch planetary ball-mill with agate jars.

Rippled smear slides for calcareous nannoplankton were prepared and permanently mounted with optical cement (Entellan) following the procedure described in Johnson et al. (2012). Slides were observed using the optical petrographic microscope Ortholux II-Pol under 1250 magnification. Calcium carbonate in sediment was determined using an Eijkelkamp calcimeter

3.2.1 Radiocarbon dating

Six samples (retrieved at 153cm, 201cm, 355cm, 553cm, 625.5cm and 636cm) were selected for AMS radiocarbon dating and processed at Beta Analytic (USA) laboratories. Radiocarbon ages determined for the organic samples were calibrated using Clam 2.2 software (Blaauw, 2010) and the IntCal13 calibration curve (Reimer et al., 2013). Sedimentation rates were extrapolated using CLAM 2.2 software (Blaauw, 2010).

3.2.2 Magnetic susceptibility

Volume magnetic susceptibility (MS) was measured in SI units directly over the core at every 2cm using a Bartington® MS2 instrument equipped with a MS2C 100mm diameter ring sensor. Measured values were corrected for drift and diameter following Bartington's operation manual OM1131. MS measurements were initiated 1.7cm below the core top in order to match the MS2C ring centre with each corer at a centimetre level, being this difference corrected for plotting.

3.2.3 Grain-size and compositional analysis

Total sediment grain-size distribution was measured in basically muddy sediment by laser diffraction using a Malvern Mastersizer 2000. Samples were previously washed with tap water and passed through a 1mm-mesh sieve. The fraction >1mm was determined and total grain-size distribution recalculated. Coarse sediment samples were washed through a 63μm-mesh sieve and the <63μm fraction was measured by laser diffraction. The fraction >63μm was weighted and total grain-size distribution recalculated. The coarse fraction was described using a Leica MZ12 binocular stereomicroscope to characterise composition and morphoscopic characteristics.

3.2.4 Organic chemistry

Total organic matter content (OM_T) was determined following Kristensen (1990) adapted method *Loss on ignition* (LOI): samples were heated in a muffle furnace at 520ºC for 6h and OM_T determined by weight difference.

Total organic carbon (%C_{org}), total nitrogen (%N) and $\delta^{13}C_{VPDB}$ were determined from sediment collected from the bank of the present-day river channel and the Arapouco core at every 10cm. A higher resolution was used in core sections yielding significant differences in other measured proxies, particularly MS. The analyses were done in ground sub-samples after removal of inorganic carbon using HCl 10%. All samples were processed at *Servizos de Apoio a Investigación*, University of A Coruña (UDC), Spain. Samples were homogenized and weighed in tin capsules. Capsulated samples were analysed with a FlashEA1112 combustion elemental analyser (ThermoFinnigan) coupled on−line with a Delta Plus Finnigan MAT Isotope Ratio Mass Spectrometer. All carbon and nitrogen isotope ratios are expressed in conventional δ notation: $\delta^{13}C_{VPDB} = \delta^{15}N_{AIR}$ [($R_{sample} = R_{standard}$)] 1000, where R_{sample} and $R_{standard}$ are the $^{13}C/^{12}C$ or $^{15}N/^{14}N$ isotope ratios of the sample and standard, respectively. The $\delta^{13}C$ isotope ratio of samples was determined by comparison with a CO_2 reference gas standard (99.996%, $\delta^{13}C_{VPDB}$ = -6.317) and values are reported relative to Vienna Pee Dee Belemnite (VPDB) standard.

3.2.5 Diatom identification

Twenty-four samples were analysed for diatom identification. Diatoms are extremely sensitive to salinity, sediment availability and hydrodynamic conditions, factors that control the evolution of coastal water bodies (e.g., Cooper, 1999, Denys and De Wolf, 1999) providing evidence of process-response thresholds controlled by local factors. Sediment samples (0.01g dry weight) were processed according to standard techniques (Renberg, 1990). Cleaned subsamples were dried onto coverslips and mounted onto microscope slides with Naphrax (RI = 1.74). Identification was undertaken with a magnification of 1000x using a Nikon Eclipse 600 microscope with Nomarski differential interference contrast optics. A minimum of 300 valves were counted per sample. Interpretation was based on the diatom species (with relative abundances equal to or higher than 5% in at least one sample), environmental preferences (salt, brackish or fresh water), habitat and lifeform (benthic, thycoplanktonic or planktonic), following Vos and De Wolf (1993).

4. Results

4.1 Chronology

Table 2 shows results obtained from radiocarbon dating of Arapouco core. With exception of the date obtained at 153cm depth, all other radiocarbon age values fall within the interval of 3400-3100 yr BP. A mean SR of 2.2cm yr^{-1} was determined using CLAM (Blaauw, 2010), representing a high sedimentation rate in a short time interval (Fig. 2). The mean SR of 0.06cm yr^{-1} was determined for the last 3232 years (Fig.2).

Table 2 – Radiocarbon dating results. BP ages were calibrated with Clam 2.2 software (Blaauw, 2010) using the calibration curve IntCal13 (Reimer et al., 2013).

Figure 2 - ^{14}C BP dates and age model with representation of the samples used for ^{14}C dating done with Clam 2.2 software (Blaauw, 2010). and using the IntCal13 calibration curve (Reimer et al., 2013).

The date obtained for the sample Arapouco3#4 552-554 was not used on the SR model because presents an older date than the values obtained for the samples at the base of the core (samples Arapouco3#5 635-637 and Arapouco3#5 624-627). The stratigraphic inversion at 553cm is possibly the result of the presence of old organic material brought to the area by the fluvial network during intense fluvial episodes (see discussion section 5.3).

4.2 Sediment units

Five sediment units were identified considering changes in the analysed proxies (Fig. 3). The interval of deposition was determined in the context of the proposed age-model. All samples prepared for calcareous nannofossils were completely barren. Calcium carbonate results indicate null or negligible amounts (<1% on the analysed samples).

Unit 1 (at the bottom, below -425cm *msl*; deposited before ca.3570 cal. BP) consists primarily of heterometric sand, mainly composed by angular to sub-angular hyaline and milky quartz (ca.99%) and mica grains. Rare lithoclasts occur.

Unit 2 (-425cm to -350cm *msl*; deposited between ca.3570 cal. BP and ca.3400 cal. BP) is characterized by MS values between $13x10^{-5}$ (SI) and $34x10^{-5}$ (SI) with the highest values corresponding to two peaks (at 415 and 407cm *msl*; Fig. 3) and related to two sand lenses observed between 407-409cm and 413-415cm *msl*. The sand (sediment >63μm) from these two layers is composed of ca.99% of hyaline and white quartz grains and in the fraction >1.4mm charcoal fragments were observed. Apart from these two coarser samples, the sediment is essentially muddy (mean values of 91%; 64% silt and 27% clay; 9% sand; Fig. 3) with OM_T values of 8% (min. 7%; max. 9%) with a single exception collected between the sandy lenses (-411cm *msl*) where OM_T shows values of ca.5%. The sand from the muddy samples is also composed by heterometric hyaline quartz (ca.99%) and mica. Vegetal and charcoal fragments were observed. Rare forms of

Actinoptychus spp were also found. Organic carbon presents mean values of 2%, C/N ratio varies between 11 and 12.5 (mean value of 11.5) and $\delta^{13}C$ shows mean values of -24‰ (Fig. 3).

At the top of this Unit (-354 to -351cm *msl*) a whole shell of *Scrobicularia plana* was found. The diatom record is mainly composed by marine to marine/brackish planktonic taxa such as *Paralia sulcata* and *Actinoptychus senarius*, although some epiphytic and epipelic diatoms of brackish character (as *Cocconeis placentula* and *Epithemia adnata*) also occur (Diatom Association Zone (DAZ) 1; Fig. 4).

Figure 3 - Representation of sedimentological and organic proxies against depth below surface and height: magnetic susceptibility (MS), texture, total organic matter (OM_T), organic carbon (C_{org}), total nitrogen (N), C/N and $\delta^{13}C$. The black line represents results obtained from Arapouco3 and the grey line results from Arapouco2 sections. Both present the same behaviour in the overlapping region. Grey bars in MS profile represent higher inputs of terrestrial material (see discussion below). The black arrow indicates the decreasing trend of $\delta^{13}C$ upcore.

Unit 3 (-350cm to -130cm *msl*; deposited between ca.3400 cal. BP and 3300 cal. BP) shows the lowest MS values in Arapouco core (average MS of $12x10^{-5}$ (SI), min. of $10x10^{-5}$ (SI) and max. of $15x10^{-5}$ (SI); Fig. 3). Sediment mostly consists of mud (average 85%; 60% silt and 25% clay) with ca.15% of sand. The sand is composed of very fine, slightly heterometric, hyaline quartz grains (ca.99%) and mica. Similarly, with Unit 2, vegetal and charcoal fragments were observed, and rare *Actinoptychus* spp specimens were identified. Total OM is ca.8% (Fig.2; min. 6.6%, max. 9.1%). Organic carbon presents mean values of 2%, mean C/N ratio of ca.12, with higher values at the base of the unit (ca.13.7%). Values for $\delta^{13}C$ are virtually invariant in this unit, averaging -24‰.
A whole shell of *S. plana* was found at -295cm *msl*, and the diatom assemblage contains almost exclusively marine planktonic diatoms (DAZ 2; Fig.4) *Thalassiosira* species associated with other brackish epipelic and epiphytic taxa such as *Gyrosigma* spp and *Mastogloia* spp. The presence of the marine planktonic *Thalassionem nitzschioides* is noticeable.

Figure 4 – Down-core distribution of selected diatom taxa and diatom-assemblages zones (DAZ) in the sediment record plotted against core depth and *msl* height.

An increase in MS characterizes Unit 4 (-130cm *msl* to *msl*; deposited between ca.3300 cal. BP and 3240 cal. BP), the susceptibility profile showing regularly spaced MS peaks (MS average $17x10^{-5}$ (SI) and MS maxima at -108cm *msl* ($37x10^{-5}$ (SI)) and -18cm *msl* ($31x10^{-5}$ (SI), min. $9x10^{-5}$ (SI));

Fig.3). The sediment is essentially muddy (average 90%; 60% silt and 30% clay; 10% sand). The particles with sand dimension (>63μm) correspond to coarse vegetal fragments. Rare quartz grains were observed. Total OM presents mean values of 8.4%, C_{org} is of 2.4% and C/N ratio increases from 12 at the base of the unit to 14 at *msl*. $\delta^{13}C$ varies between -24.5 and -26‰ decreasing upwards (Fig.3).

In the case of the diatom content, the most significant feature in this unit is the reduction of the previously dominant marine planktonic diatoms and the increase in the proportion of brackish/freshwater to freshwater taxa (DAZ 3; Fig. 4). The transition is mainly characterized by marine, marine/brackish and brackish/freshwater diatoms, with *Cocconeis* spp and *Nitzschia* spp as dominant species. The dominance of epiphytic diatoms suggests shallow water with abundant macrophytes. Similarly, the dominance of *Cocconeis* spp and *Nitzschia* spp associated with *Cyclotella* sp. aff. *meneghiniana* suggests brackish conditions. Marine/brackish to brackish epipelic diatom assemblages associated with species such as *C. placentula* also occur in this unit.

Unit 5 (*msl* to 220cm *msl*; after 3240 cal. BP) represents the 2 uppermost meters of Arapouco core. It is characterized by MS values between $4.5\text{x}10^{-5}$ (SI) and $38\text{x}10^{-5}$ (SI) with the lower values ($4.5\text{x}10^{-5}$ and $10\text{x}10^{-5}$ (SI)) measured in the top 10cm (Fig. 3). MS peaks occur between 112cm and 100cm *msl* (maximum value of $38\text{x}10^{-5}$ (SI)) and between 146cm and 182cm with values of ca. $27\text{x}10^{-5}$ (SI). The sediment is mostly composed of mud (averaging 87%; 58% silt and 29% clay; 13% sand; Fig.3). However, above 100cm the content in sand increases: a peak in sand proportion was found at ca.80cm (ca.22% of sand) and in the topmost 30cm and constitutes ca.50% of the total sediment. The coarse fraction (>63μm) corresponds to sand <1mm and is mainly composed of quartz grains. Iron oxides are frequent among the sand. Total OM gradually decreases upwards, presenting mean values of ca.5% (min. of 2.7 and max. of 6.3%; Fig.2). Organic carbon shows the lowest values found in the core with mean values of 0.8%. The three upppermost samples show an increase in C_{org} from 1% to 2.4% at the very top sample. Between 0m *msl* and 110cm *msl* a marked decrease in the C/N ratio (mean value of. 6.6) is observed, related with the decrease in the proportion of C_{org} (N_{Tot} is almost constant). From 110cm *msl* to the top of the core C/N ratios show values around 10. $\delta^{13}C$ values vary between -25 and -27‰ with lower values at the top. In this unit the diatom record is mostly composed of fragments, making the identification of correspondent species impossible.

5. Discussion

5.1 Source of organic material

Estuarine sediments incorporate organic materials and compounds from both aquatic and terrestrial organisms that were drained and transported to the depositional area via the hydrographic network (Lamb et al., 2006). In this work, all source-sensitive organic indicators (i.e., C_{org}, N_{Tot}, $\delta^{13}C$) show that Units 2, 3 and 4 are different from Unit 5 in what concerns the origin of organic material incorporated in sediment (Fig.3).

Considering that OM_T displayed a mean value of 8.5% (max=10%; min=7%) in Units 2 to 4 and that the mean value of OM_T is of 5% in Unit 5 (max=8%; min=3%) there is a clear indication of a shift in the organic matter input from 0m *msl* upwards (Fig.3). Figures 5a and 5b show the correlation between OM_T *vs.* N_{Tot} and OM_T *vs.* C_{org}, respectively. In Units 2, 3 and 4 (i.e., below 0m *msl*) OM_T correlates with N and C_{org} (r^2=0.55, n=49, considered significant for p=0.05 using F-test in both cases) suggesting that both organic elements share a similar origin and vary in agreement with the OM_T. In Unit 5 OM_T presents no correlation at all with either N (Fig. 5a) or C_{org} (Fig. 5b) suggesting that these organic elements vary independently from OM_T. In fact, OM_T decreases gradually from the base to the top of Unit 5, and both C_{org} and N decrease abruptly at the base and remain almost constant along the remnant of the unit. The decrease in the organic compounds is interpreted as related to oxidation processes that favoured the loss of these organic elements, eventually enhanced by agriculture practices including rice production.

Nitrogen and C_{org} are correlated (r^2=0.85, n=49, considered significant for p=0.05 using F-test) in Units 2, 3 and 4 and also in Unit 5 (r^2=0.86; n=9, considered significant for p=0.05 using F-test) (Fig. 5c) pointing to the same source of both organic components in these units. Three anomalous N values were measured between 0cm and 100cm *msl* that are most probably related to additional inputs of N-fertilizers associated with rice production.

Figure 5 – Correlation between: a - OM_T and N_{Tot}; b - OM_T and C_{org}; c - N_{Tot} and C_{org} (c). Black diamonds represent samples from Units 2, 3 and 4 and grey squares represent samples from Unit 5. Black triangles (c) represent samples enriched in N_{Tot}.

$\delta^{13}C$ is widely used to determine the origin of the organic matter stored in the sediment (e.g., Lamb et al., 2006). Generally, terrestrial and freshwater organic materials present lower $\delta^{13}C$ values than marine organic components (Lamb et al., 2006 and references therein). $\delta^{13}C$ decreases from the core base to the top (-23‰ to -27‰), with mean $\delta^{13}C$ values of -24‰ in Units 2 and 3, -25‰ in

Unit 4 and -26‰ in Unit 5. This change reflects an increase of the contribution of organic matter from terrestrial plants and freshwater phytoplankton to the sediment through time.

Lamb et al. (2006 and references therein) also compiled data of studies investigating the value of $\delta^{13}C$ and C/N ratios to identify sources of organic matter in intertidal wetland sediment. To the best of our knowledge, there are no previous studies on the origin of organic matter in sediments accumulated in the study area in both present-day times and throughout the recent past. To overcome this drawback, $\delta^{13}C$ and C/N data from Arapouco core were plotted in Lamb et al.'s chart (2006; Fig.6). The organic material of Units 2, 3 and 4 represent a mixture between marine dissolved organic carbon (marine DOC; Fig.6) and carbon sourced in C3 terrestrial plants and freshwater dissolved organic carbon (freshwater DOC; Fig.6). Units 2 and 3 sediments received a higher contribution of marine DOC (Fig.6), reflecting estuarine conditions with higher marine influence. Within Unit 4 the contribution of freshwater DOC and C3 terrestrial plants (Fig. 6) increases, pointing to a higher contribution of freshwater/terrestrial organic materials. C/N *vs.* $\delta^{13}C$ in Unit 5 indicate a shift to organic material originated in freshwater components, initially essentially freshwater DOC and later freshwater particulate organic carbon (POC) and algae (Fig. 6).

Figure 6 – C/N vs. $\delta^{13}C$ results plotted at adapted Lamb et al.'s graph (2006). Black filled squares represent Unit 2; black triangles represent Unit 3; black crosses represent Unit 4, and black diamonds represent Unit 5. The black circle represents the sediment collected in the main channel at Arapouco in 2017.

Based in our data, one can assume that the organic material is typical of an estuarine area, with contributions from both terrestrial/freshwater and marine organic compounds, between the core base (ca.425cm *msl*) and 0m *msl*, corresponding to Units 2, 3 and 4 previously described. The basal units (Units 2 and 3) reflect the higher influence of marine water and Unit 4 seems to reflect the transition to a more terrestrial/freshwater influenced environment. Above 0m *msl* (Unit 5) organic material shows a higher contribution of freshwater phytoplankton, which is consistent with the aggradation of an alluvial plain. The existence of *S. plana* shells considered to be *in situ* in Units 2 and 3 are also indicative of prevailing estuarine conditions (tidal flat or high subtidal zone) in this area.

5.2 Fluvial *versus* marine influence and palaeoecology of diatoms

Together with the organic material analysis, palaeoenvironmental interpretations herein are also based on major trends of the relative abundance of diatom autoecological groups. Marine tychoplankton and plankton dominate the sedimentary sequence of the Arapouco core (Fig. 4). Marine plankton accompanied by brackish epipelon dominates the core base. Marine plankton increases towards the middle of the sequence and marine, brackish epipelon and epiphytic diatoms also increase further up the sequence. These can be used to characterize different tidal sub-environments. *Thalassiosira decipiens* is very abundant in the Arapouco sedimentary sequence (Fig. 4). *T. decipiens* is a diatom that shows a more coastal than planktonic behavior that frequently appears throughout the present-day estuary with its highest development during the winter-early spring period with polihaline conditions (Coutinho, 2003). It has been reported from vast inland seas, estuaries, bays, shallow coastal waters and rivers with tidal influence (Hasle and Sylversten, 1996) and is especially abundant in tidal inlets and large tidal channels (Vos and De Wolf, 1988). This broad distribution through rivers, estuaries, inland salt waters, and marine localities, suggests an ecologically diverse and tolerant taxon. Tide transported planktonic diatoms are often found in tidal-channel and tidal-inlet sediments (Vos and De Wolf, 1993). In these environments, the conditions of high current velocities and poor light do not favour the development of diatom populations on the sediments (benthic and epiphytic groups) (Anderson and Vos, 1992).

The increase in abundance of *Cyclotella meneghiniana*, a brackish/freshwater planktonic species, at the bottom of the diatom record correlates well with the reconstructed increase in freshwater influence in the estuarine environment (Unit 2; DAZ 1; Fig. 4). Its decrease at Unit 3 (DAZ 2; Fig. 4) may be indicative of reduced allochthonous input from upstream, and indicative of reduced tidal mixing. This trend reverses in the upper section of the core (Unit 4; DAZ 3; Fig. 4) where *T. decipiens* decreases and *C. meneghiniana* increases indicating a decline in salinity that could be caused by a stronger freshwater influence and increasing eutrophication (Weckström, 2006).

Most of the benthic community consists of epipelic and epiphytic diatoms at this time (Fig. 4). *Nitzschia sigma* is an epipelic taxon, dominant at the top of the sequence (Unit 4; DAZ 3; Fig. 4). It usually appears in high proportions within the intertidal zone or (shallow) subtidal zone in salinities of 5-17‰ and adapted to higher turbidity (Coutinho, 2003). Brackish epiphyte taxa are significant towards the top of the core. Accompanied by marine plankton, these assemblages are characteristic of mudflats; they live on macroalgae and waterplants. They are characteristic of low-energy environments that are permanently submerged (Vos and De Wolf, 1993).

Higher marine influence in the innermost and marginal areas of the estuary can be triggered by sea-level oscillations, storminess episodes, tsunami events or changes in river flow. Which forcing was more decisive to explain such higher marine influence is open to question.

During the time span corresponding to the deposition of sediments in Arapouco, the sea level was rising at a slow rate (e.g. Vis et al., 2008, Leorri et al., 2012, Costas et al., 2016a; García-Artola et al., 2018) of ca.0.31 ± 0.02 mm yr^{-1} (Costas et al., 2016a). Long-term regional oscillations of the relative sea level can be brought about by changes in the wind regime, ocean heat, freshwater content and atmospheric pressure (Church et al., 2013). Costas et al. (2016a) reported small oscillations of the sea level rise curve in the last 6500 cal. BP in the Sado area, most probably associated with climate variability, which induced a small positive change of the sea level ca.3600 cal. BP (Costas et al., 2016a). Also, an enhanced storminess period affecting southern Europe, and particularly the Western Portuguese central coast, SW France coast and the western Mediterranean seems to have occurred in the time interval of 4000-3000 cal. BP (Costas et al., 2016b and references therein). Costas et al. (2015) mentioned an episode of shoreline retreat at the Tróia spit ca.4000 cal. BP and, according to these authors, the barrier enclosing the Sado estuary was much less robust until ca.3250 cal. BP. High-energy events were recorded at the Guadalquivir estuary/sandy barrier at 4000 cal. BP, 3550 cal. BP and 3150 cal. BP (Rodríguez-Ramírez et al., 2015). Both 4000 cal. BP and 3150 cal. BP events were correlated with storminess conditions, but the 3550 cal. BP event was related to a seismic event that occurred at the SW Portuguese margin cataloged by Lario et al. (2011) as a tsunami-generated event (Rodríguez-Ramírez et al., 2015). However, evidence for this event has only been reported in some areas of the Gulf of Cadiz, and it was considered as a seismic event that generated a local tsunami (Lario et al., 2011). Also, evidence of barrier permeability and an increase of marine influence around this period were found on sedimentary sequences sampled along the SW Portuguese coast at Albufeira, Melides and Santo André coastal lagoons (Fig. 1): Albufeira lagoon between 4900 and 3400 cal. BP; Melides lagoon after 3950 cal. BP; and Santo André lagoon between 3770 and 1500 cal. BP (Freitas et al., 2002).

In the case of the influence of river discharge on salinity changes in estuaries, several accounts have been published (e.g., Liu et al., 2007, Shaha and Cho, 2017, Robins et al., 2018). For the north Portuguese estuaries, the results point to an increase in salinity during periods with low river flows (Douro estuary - Azevêdo et al., 2010; Mondego estuary - Baptista et al., 2010). For the Tagus estuary, although variation in salinity over the estuarine area for wet (>300m^3 s^{-1}) and dry (<300 m^3 s^{-1}) years has not been published, a higher density of marine occasional species has been reported in the dry years for the upper estuary (Costa et al., 2007) probably reflecting higher salinity conditions. For the Sado estuary, no data was available until now but, at present, due to the low river discharge, as a consequence of the flow control (water retention by dams) and the severe drought felt in Portugal during 2017, the marine influence is present in the channel at Arapouco, where organic matter is represented by Marine POC and Marine algae (Fig. 6) (Index SPI 12 months, http://www.ipma.pt/pt/oclima/observatorio.secas/spi/monitorizacao/situacaoatual/; February 2018). Drier climatic conditions were defined for the northern littoral area of Alentejo (south Portugal) during the Late Holocene, based on palaeoecological analysis of sediment cores collected on littoral lagoons and peat bogs (Queiroz, 1999). The drier conditions were also reconstructed for other geographical areas of SW Europe (e.g., Fletcher et al., 2007; Carrión et al., 2010; Danielsen et al., 2012; Fletcher et al., 2013; Chabaud et al., 2014). In SW Portugal the drier conditions led to meager sedimentation rates estimated in peat bogs at the SW Portuguese coast, such as Poços do Barbaroxa (Fig.1; Leira et al., accepted for publication).

Could a climate-driven, small impulse of the sea level and low river flow discharges, associated with drought periods, promote a higher marine influence at the marginal and innermost areas of the estuary?

Published data point to long-term drier conditions during the Late Holocene on SW Iberia (e.g., Chabaud et al., 2014), particularly an aridification event between 3700-2900 cal. BP on Mediterranean Iberia (e.g., Fletcher et al., 2013), but also to the onset of a storminess period possibly leading to positive oscillations in sea level (Costas et al., 2016a). Most probably the higher marine influence registered at Arapouco between 3400 cal. BP and 3300 cal. BP is related to lower river discharges derived from drier climatic conditions during this period. However, storminess conditions, probably defined by very intense, but infrequent, storms and the associated positive sea-level oscillation recorded at ca.3600 cal. BP could also have played a role, allowing the intrusion of marine water upriver, particularly under low river flows.

5.3 High sedimentation rates and sedimentation constraints

Sedimentation rates (SR) of ca.2.2cm yr^{-1} between 685-600 cal. BP and of 0.13cm yr^{-1} for the last 1350 years were determined in a core collected at the Sado saltmarsh near Alcácer do Sal (Moreira, 2016). In the Arapouco core, a mean SR of ca.2.2cm yr^{-1} between ca.3570 and 3240 cal. BP (Units 2, 3 and 4) and a SR of 0.06cm yr^{-1} after the youngest radiocarbon age (in Unit 5), were determined, values that are in the same order of magnitude although slightly lower than in Alcácer do Sal.

The higher SR calculated in the study area is high when compared with the mean SR values determined for the Tagus estuary. An average SR of 0.19cm y^{-1} was established for the top ca.6m of the VAL core (Vis et al., 2015), collected ca.80km upstream of the Tagus outlet, representing a sequence of sedimentation of brackish marshes and tidal flats at the base (Unit 3A; Vis and Cornelius, 2009) in the last ca. 3500 cal BP overlaid by fluvial deposits (Unit 6B; Vis and Cornelius, 2009).

What conditions could have promoted high-sedimentation rates at the inner Sado estuary, considering the drier climatic conditions and the time interval between ca.3570 cal. BP and 3240 cal. BP?

Estuarine areas are susceptible to variations on river discharge, flooding and sediment supply (e.g., Brown, 1997). Accommodation space also controls sedimentation rates. Despite general drier conditions at the beginning of the Late Holocene that could increase the sediment availability due to vegetation retreat, storminess periods were documented on the NW Mediterranean (e.g., Sabatier et al., 2012), southern Spain (e.g., Rodríguez-Ramírez et al., 2015) and along the Portuguese coast (e.g., Costas et al., 2015).

Wetter and warmer conditions that favour pedogenesis and increase transport of magnetic particles from the parent soil to the proximal hydrographic basin will translate in to a higher MS signal in the sediment (e.g., Ellwood et al., 2001). In the case addressed here, higher precipitation will increase the river transport competence allowing for the higher proportion of magnetic particles sourced from the Iberian Pyrite Belt to reach and accumulate in the core sediment.

Several MS peaks are present, particularly at Units 2, 4 and 5 (Fig. 3) as a response to episodes of intensification of terrestrial input, likely favored by short episodes of intense precipitation.

During the deposition of Unit 2 higher intensity MS peaks (Fig. 3) at the base point to higher inputs of terrigenous material. In this Unit, the MS peaks correspond to the occurrence of coarse (sandy) sediment layers mostly constituted by quartz grains brought to the area by the fluvial network. Quartz is a diamagnetic mineral (Hayes, 2015) and thus responds to magnetization yielding negative values. Iron-coating on the sand grains were not observed in morphoscopic analysis of samples, and it is reasonable to conclude that the peaks in MS are probably related to the finer constituents (size fraction <63μm).

Despite the contribution of terrigenous material to this area, organic material is primarily derived from an estuarine area (inner estuary) considering the marine DOC as the main source for the organic carbon.

Alternatively, Unit 3 is characterized by lower MS values (Fig. 3), suggesting lower terrestrial inputs at this time. Both the higher marine influence and the lower terrigenous contribution during accumulation of Unit 3 seem to reflect the retreat of the fluvial-estuarine boundary to riverine reaches upstream of its present-day location.

In Unit 4 several MS peaks were identified reflecting higher terrigenous inputs with high frequency (each ca.50cm). The origin of the OM points to higher contributions of terrestrial/freshwater organic material reflecting the transition to a terrestrial/freshwater environment, with the fluvial-estuarine transition boundary advancing downstream. Unit 4 deposited before ca.3240 cal. BP, and the top of the Unit corresponds to present *msl*. Assuming a sea-level rise rate of 0.31mm y^{-1} (Costas et al., 2016a) the *msl* at that time was ca.1m below present and considering tidal characteristics similar to the existent today, the deposition of Unit 4 has occurred under intertidal conditions. The high terrigenous input and the high SR promoted the fast silting-up of the area and the transition from an aggradational subtidal-intertidal mudflat to an alluvial plain.

Unit 5 corresponds to the aggradation of the alluvial plain considering the low OM content and its enrichment in freshwater components. Several MS peaks were obtained on this Unit reflecting higher inputs of terrigenous material with higher contents of coarse material in the top 100cm. The observed low SR for Unit 5 is probably related with the silting up of the area and the decrease of accommodation space: the sedimentation being mostly dependent on repetitive fluvial flooding. Similarly to the Arapouco core, the high SR determined during the 13^{th} and 14^{th} centuries in the Alcácer do Sal core (Moreira, 2016) could correspond to high terrestrial inputs promoting the silt-up of this subtidal area. The decrease in the sedimentation rate for the top sections of the core (>40cm *msl*) could be related to the higher altitude and reduction of the accommodation space forming conditions for the development of a saltmarsh.

6. Conclusions

The Sado estuary has experienced significant changes in the fluvial-estuarine boundary during the Late Holocene, and particularly between ca.3570 cal. BP and 3240 cal. BP. During this period (that lasted for about 300 years) high-sedimentation rates (mean SR of ca.2.2cm yr^{-1}) and changes on the primary source of sediment might reflect changes on the precipitation regime and, to a much lesser extent, regional oscillations in sea level related to climate variability.

Between the core base (ca.-400cm *msl*; 3570 cal. BP) and the 0m *msl* (3240 cal. BP), the Arapouco sediments were influenced by marine/brackish water with a high contribution of marine contents to the OM. The sedimentation in the area is compatible with an intertidal flat (Unit 2). The estuarine-fluvial boundary retreated upstream for ca.100 years (Unit 3).

The marine influence decreased at Unit 4 while fluvial/terrestrial influence increased in the sedimentation pattern. The deposition of Unit 4 took place in the intertidal zone under high contribution of terrigenous materials. The high SR promoted the fast silting-up of the area and the aggradation of an alluvial plain took place above *msl* (Unit 5). The high SR rates calculated at Alcácer do Sal show that the sediment depocenter migrate downstream after filling of the accommodation space at Arapouco.

On a broader perspective, the Sado estuary revealed to be a source of information concerning climate variability and sea level oscillations during the Late Holocene. The high sedimentation rate found in this estuary allowed to reconstruct the environmental evolution at high resolution, using a suite of environmental-sensitive proxies. Results and paleoenvironmental inferences obtained and discussed herein, can be applied to similar coastal landscapes located elsewhere in the western Iberian coast.

Acknowledgments

This work was developed in the scope of a BD grant funded by FCT (SFRH/BD/110270/2015) and under projects CoChange (HAR2014-51830-P), and COASTTRAN (HAR2011-29907-C03-00) financed by the Spanish Ministry of Science and Innovation and project Back to Sado (PTDC/HIS-ARQ/121592/2010) funded by FCT. The authors would also like to acknowledge the support of the Instituto Dom Luiz - IDL (UID/GEO/50019/2013).

We would like to thank Santa Casa da Misericórdia de Alcácer do Sal and Eng. Custódio Lutas who made possible the recovery of Arapouco core on Herdade de Arapouco. We would also like to thank Alexandra Amorim, Randi Danielsen, Tiago Silva and Vera Lopes who helped on the core collection.

References

Anderson NJ and Vos P (1992) Learning from the past: diatoms as palaeoecological indicators of changes in marine environments. *Netherlands Journal of Aquatic Ecology* 26(1): 19-30.

Antunes M, Pais J, Gonçalves F, Oliveira J, Peleja AF, Barroso JP, Romão JA, Lopes JC, Casimiro J (1991) Carta Geológica de Portugal 1:50000 Folha 39-D Torrão.

Azevêdo IC, Bordalo AA, Duarte PM (2010) Influence of river discharge patterns on the hydrodynamics and potential contaminant dispersion in the Douro estuary (Portugal). *Water Research* 44: 3133-3146.

Baptista J, Martinho F, Dolbeth M, Viegas I, Cabral H, Pardal M (2010) Effects of freshwater flow on the fish assemblage of the Mondego estuary (Portugal): comparison between drought and non-drought years. *Marine and Freshwater Research* 61: 490-501.

Bettencourt A, Gomes V, Dias A, Ferreira G, Silva M, Costa L (2003) *Estuários Portugueses*. Lisboa: Direcção dos Serviços de Planeamento, Instituto da Água, Ministério das Cidades, Ordenamento do Território e Ambiente.

Blaauw M (2010) Methods and code for ‘classical’ age-modelling of radiocarbon sequences. *Quaternary Geochronology* 5(5): 512-518.

Brito P (2009) *Impactos da elevação do nível médio do mar em ambientes costeiros: o caso do estuário do Sado*. PhD thesis, Departamento de Geologia da Faculdade de Ciências, Universidade de Lisboa, Portugal.

Brown AG (1997) *Alluvial geoarchaeology. Floodplain archaeology and environmental change*. Cambridge Manuals in Archaeology.

Carrión JS, Fernández S, González-Sampériz P, Gil-Romera G, Badal E, Carrión-Marco Y, López-Merino L, López-Sáez JA, Fierro E, Burjachs F (2010) Expected trends and surprises in the Lateglacial and Holocene vegetation history of the Iberian Peninsula and Balearic Islands. *Review of Palaeobotany and Palynology* 162: 458-475.

Chabaud L, Sánchez Goñi MF, Desprat S, Rossignol L (2014) Land–sea climatic variability in the eastern North Atlantic subtropical region over the last 14,200 years: Atmospheric and oceanic processes at different timescales. *The Holocene* 24: 787-797.

Church JA, Clark PU, Cazenave A, Gregory JM, Jevrejeva S, Levermann MA, Merrifield MA, Milne GA, Nerem RS, Nunn PD, Payne AJ, Pfeffer WT, Stammer D, Unnikrishnan AS (2013) Sea Level Change. In: Stocker TF, Qin D, Plattner G-K, Tignor M, Allen SK, Boschung J, Nauels A, Xia Y, Bex V, Midgley PM (eds.) *Climate Change 2013: The Physical Science Basis. Contribution of Working Group I to the Fifth Assessment Report of the Intergovernmental Panel on Climate Change*. United Kingdom and New York, USA: Cambridge University Press, pp. 1137-1216.

Colman SM, Baucom PC, Bratton JF, Cronin TM, McGeehin JP, Willard D, Zimmerman AR (2002) Radiocarbon dating, Chronologic Framework, and Changes in Accumulation Rates of Holocene Estuarine Sediments from Chesapeake Bay. *Quaternary Research* 57: 58-70.

Cooper SR (1999) Estuarine palaeoenvironmental reconstructions using diatoms. In: Stoermer, E.F. and Smol, J.P. (eds.) *The diatoms: applications for the environmental and earth sciences*. Cambridge: Cambridge University Press, pp. 352-373.

Costa MJ, Vasconcelos R, Costa JL, Cabral HN (2007) River flow influence on the fish community of the Tagus estuary (Portugal). *Hydrobiologia* 587: 113-123.

Costa AC and Soares A (2009) Trends in extreme precipitation indices derived from a daily rainfall database for the South of Portugal. *International Journal of Climatology* 29: 1956-1975.

Costas S, Rebêlo L, Brito P, Fitzgerald D (2015) The Joint History of Tróia Península and Sado Ebb-Delta. In: Randazzo G, Jackson DWT, Cooper JAG (eds.) *Sand and Gravel Spit*. Spinger, pp. 79-102.

Costas S, Ferreira O, Plomaritis TA, Leorri E (2016a) Coastal barrier stratigraphy for Holocene high-resolution sea-level reconstruction. *Scientific Reports* 6: 38726.

Costas S, Naughton F, Goble R, Renssen H (2016b) Windiness spells in SW Europe since the last glacial maximum. *Earth and Planetary Science Letters* 436: 82-92.

Coutinho MTP (2003) *Comunidade fitoplanctónica do estuário do Sado. Estrutura, Dinâmica e Aspectos Ecológicos*. IPIMAR research Thesis.

Danielsen R, Castilho AM, Dinis PA, Almeida AM, Callapez PM (2012) Holocene interplay between a dune field and coastal lakes in the Quiaios-Tocha region, central littoral Portugal. *The Holocene* 22(4): 383-395.

Denys L and De Wolf H (1999) Diatoms as indicators of coastal paleoenvironments and relative sea-level change. In Stoermer EF and Smol JP (eds.) *The diatoms: applications for the environmental and earth sciences*. Cambridge, Cambridge University Press, pp. 277-297.

Diniz M and Arias P (2012) O povoamento humano do paleo-estuário do Sado (Portugal): Problemáticas em torno da ocupação dos concheiros Mesolíticos. In: Almeida AC, Bettencourt AMS, Moura D, Monteiro–Rodrigues S, Alves MIC (eds.) *Mudanças ambientais e interação humana na fachada atlântica ocidental*. Coimbra: APEQ/CITCEM/CEGT/CGUP/CCT, pp. 139-157.

Ellwood BB, Harrold FB, Benoist SL, Straus LG, Morales MG, Petruso K, Bicho NF, Zilhão J, Soler N (2001) Paleoclimate and intersite correlations from Late Pleistocene/Holocene cave sites: Results from Southern Europe. *Geoarchaeology: An International Journal* 16 (4): 433-463.

Fletcher W, Borki T, Moura D (2007) Palynological evidence for environmental and climatic change in the lower Guadiana valley, Portugal, during the last 13000 years. *The Holocene* 17 (4): 481-494.

Fletcher WJ, Debret M, Sanchez Goñi MF (2013) Mid-Holocene emergence of a low frequency millennial oscillation in western Mediterranean climate: Implications for past dynamics of the North Atlantic atmospheric westerlies. *The Holocene* 23: 153-166.

Freitas MC, Andrade C, Cruces A (2002) The geological record of environmental changes in southwestern Portuguese coastal lagoons since the Lateglacial. *Quaternary International* 93-94: 161-170.

García-Artola A, Stephan P, Cearreta A, Kopp RE, Khan NS, Horton BP (2018) Holocene sea-level database from the Atlantic coast of Europe. Quaternary Science Reviews 196: 177-192.

Gonçalves F and Antunes MT (1992) Notícia explicativa da Folha 39-D Torrão, Carta Geológica de Portugal 1:50000. Lisboa: Serviços Geológicos de Portugal.

Hasle GR and Syvertsen EE (1996) Marine diatoms. In: Tomas CR (ed.) *Identifying marine phytoplankton*. San Diego, CA: Academic Press: pp. 5–383.

Hayes WM (ed.) (2015) *CRC Handbook of Chemistry and Physics 96th Edition*. CRC press.

INE, 2007. Anuário Estatístico da Região do Alentejo, Lisboa, INE.

Index SPI 12 months, http://www.ipma.pt/pt/oclima/observatorio.secas/spi/monitorizacao/situacaoatual/; February 2018

Jiménez Cisneros BE, Oki T, Arnell NW, Benito G, Cogley JG, Döll P, Jiang T, Mwakalila SS (2014) Freshwater resources. In: Field CB, Barros VR, Dokken DJ, Mach KJ, Mastrandrea MD, Bilir TE, Chatterjee M, Ebi KL, Estrada YO, Genova RC, Girma B, Kissel ES, Levy AN, MacCracken S, Mastrandrea PR, White LL (eds.) *Climate Change 2014: Impacts, Adaptation, and Vulnerability. Part A: Global and Sectoral Aspects. Contribution of Working Group II to the Fifth Assessment Report of the Intergovernmental Panel on Climate Change*. Cambridge, United Kingdom and New York, NY, USA: Cambridge University Press, pp. 229-269.

Johnson ME, Baarli BG, Cachão M, Silva CM, Ledesma-Vázquez J, Mayoral E, Ramalho RS, Santos A (2012) Rhodoliths, uniformitarism and Darwin: Pleistocene and Recent carbonate deposits in the Cape Verde and Canary archipelagos. *Palaeogeography, Palaeoclimatology, Palaeoecology* 329-330: 83-100.

Kovats RS, Valentini R, Bouwer LM, Georgopoulou E, Jacob D, Martin E, Rounsevell M, Soussana J-F (2014) Europe. In: Barros VR, Field CB, Dokken DJ, Mastrandrea MD, Mach KJ, Bilir TE, Chatterjee M, Ebi KL, Estrada YO, Genova RC, Girma B, Kissel ES, Levy AN, MacCracken S, Mastrandrea PR, White LL (eds.) *Climate Change 2014: Impacts, Adaptation, and Vulnerability. Part B: Regional Aspects. Contribution of Working Group II to the Fifth Assessment Report of the Intergovernmental Panel on Climate Change*. Cambridge, United Kingdom and New York, NY, USA: Cambridge University Press, pp. 1267-1326.

Kristensen E (1990) Characterization of biogenic organic matter by stepwise thermogravimetry (STG). *Biogeochemistry* 9: 135-159.

Lamb AL, Wilson GP, Leng MJ (2006) A review of coastal palaeoclimate and relative sea-level reconstructions using $\delta^{13}C$ and C/N rations in organic material. *Earth-Science Reviews* 75: 29-57.

Lario J, Zazo C, Goy JL, Silva PG, Bardaji T, Cabero A, Dabrio CJ (2011) Holocene palaeotsunami record of SW Iberia. *Quaternary International* 242: 196-200.

Leira M, Freitas MC, Ferreira T, Cruces A, Connor S, Andrade C, Lopes V, Bao R (accepted for publication) Holocene sea level and climate interactions on wet dune slack evolution in SW Portugal. A model for future scenarios?. *The Holocene*

Leorri E, Cearreta A, Milne G (2012) Field observations and modelling of Holocene sea-level changes in the southern Bay of Biscay: implication for understanding current rates of relative sea-level change and vertical land motion along the Atlantic coast of SW Europe. *Quaternary Science Reviews* 42: 59-73.

Little S, Wood PJ, Elliott M (2017) Quantifying salinity-induced changes on estuarine benthic fauna: The potential implications of climate change. *Estuarine, Coastal and Shelf Science* 198: 610-625.

Liu W-C, Chen W-B, Cheng RT, Hsu M-H, Kuo AY (2007) Modeling the influence of river discharge on salt intrusion and residual circulation in Danshuei River estuary, Taiwan. *Continental Shelf Research* 27: 900-921.

Matos JX and Oliveira V (2003) Mina do Lousal (Faixa Piritosa Ibérica) - Percurso geológico e mineiro pelas cortas e galerias da antiga mina. IGME, *Pub. Museo Geominero*, n.2, 117-128.

Moreira S (2016) *Contributo da geoquímica e sedimentologia na caracterização de influências antrópicas em ambientes estuarinos*. PhD thesis, Universidade de Lisboa, Portugal.

Peyroteo-Stjerna R (2016) *On Death in the Mesolithic. Or the Mortuary Practices of the Last Hunter-Gatherers of the South Western Iberian Peninsula, 7th–6th Millennium BCE*. PhD thesis, Uppsala University. Occasional papers in archaeology 60.

Pimentel NLV, Pimentel, PRV, Azevêdo, TM, Andrade C, Freitas MC, Pereira DI (2001) Estudo sedimentológico e geoquímico de depósitos holocénicos do rio Sado. V REQUI / I CQPLI, Lisboa, 125-127.

Queiroz P (1999) *Ecologia histórica da paisagem do noroeste alentejano*. PhD thesis, Universidade de Lisboa.

Reimer P J, Bard E, Bayliss A, Beck JW, Blackwell PG, Bronk Ramsey C, Grootes PM, Guilderson TP, Haflidason H, Hajdas I, HattŽ C, Heaton TJ, Hoffmann DL, Hogg AG, Hughen KA, Kaiser KF, Kromer B, Manning SW, Niu M, Reimer RW, Richards DA, Scott EM, Southon JR, Staff RA, Turney CSM, Van der Plicht J (2013) IntCal13 and Marine13 Radiocarbon Age Calibration Curves 0-50,000 Years cal BP. *Radiocarbon* 55(4): 1869-1887.

Renberg I (1990) A procedure for preparing large sets of diatom slides from the sediment cores. *Journal of Paleolimnology* 4: 87-90.

Robins PE, Lewis MJ, Freer J, Cooper DM, Skinner CJ, Coulthard TJ (2018) Improving estuary models by reducing uncertainties associated with river flows. *Estuarine, Coastal and Shelf Science* 207: 63-73.

Rodríguez-Ramírez A, Pérez-Asensio JN, Santos A, Jiménez-Moreno G, Villarías-Robles JJR, Mayoral E, Celestino-Pérez S, Cerrillo-Cuenca E, López-Sáez JA, Léon A, Contreras C (2015) Atlantic extreme wave events during the last four millennia in the Guadalquivir estuary, SW Spain. *Quaternary Research* 83: 24-40.

Sabatier P, Dezileau L, Colin C, Briqueu L, Bouchette F, Martinez P, Siani G, Raynal O, Grafenstein UV (2012) 7000 years of paleostorms activity in the NW Mediterranean Sea in response to Holocene climate events. *Quaternary Research* 77: 1-11.

Santos JF, Pulido-Calvo I, Portela MM (2010) Spatial and temporal variability of droughts in Portugal. *Water Resources Research* 46: W03503.

Shaha DC and Cho Y-K (2016) Salt plug formation caused by decreased river discharge in a multi-channel estuary. *Nature Scientific Reports* 6:27176.

Schubel JR (1982) Estuarine sedimentation. In: Schwartz M (ed.) *Beaches and Coastal Geology. Encyclopedia of Earth Science*. Boston, MA: Springer.

Sousa PM, Trigo RM, Aizpurua P, Nieto R, Gimeno L, Garcia-Herrera R (2011) Trends and extremes of drought indices throughout the 20th century in the Mediterranean. *Natural Hazards and Earth System Science* 11(1), 33-51.

Vis G-J, Kasse C, Vandenberghe J (2008) Late Pleistocene and Holocene palaeogeography of the Lower Tagus Valley (Portugal): effects of relative sea level, valley morphology and sediment supply. *Quaternary Science Reviews* 27: 1682-1709.

Vis G-J and Cornelius K (2009) Late Quaternary valley-fill succession of the Lower Tagus valley, Portugal. *Sedimentary Geology* 221: 19-39.

Vis G-J, Cornelis K, Kroon D, Vandenberghe J, Jung S, Lebreiro SM, Rodrigues T (2015) Time-integrated 3D approach of late Quaternary sediment-depocenter migration in the Tagus depositional system: From river valley to abyssal plain. *Earth-Science Reviews* 153: 192-211.

Vos P and De Wolf H (1988) Methodological aspects of paleoecological diatom research in coastal areas of the Netherlands. *Geologie en Mijnbouw* 67: 31-40.

Vos PC and De Wolf H (1993) Diatoms as a tool for reconstructing sedimentary environments in coastal wetlands: methodological aspects. *Hydrobiologia* 269/70: 285-296.

Weckström K (2006) Assessing recent eutrophication in coastal waters of the Gulf of Finland (Baltic Sea) using subfossil diatoms. *Journal of Paleolimnology* 35: 571-592.

Wong PP, Losada IJ, Gattuso J-P, Hinkel J, Khattabi A, McInnes KL, Saito Y, Sallenger A (2014) Coastal systems and low-lying areas. In: Field CB, Barros VR, Dokken DJ, Mach KJ, Mastrandrea MD, Bilir TE, Chatterjee M, Ebi KL, Estrada YO, Genova RC, Girma B, Kissel ES, Levy AN, MacCracken S, Mastrandrea PR, White LL (eds.) *Climate Change 2014: Impacts, Adaptation, and Vulnerability. Part A: Global and Sectoral Aspects. Contribution of Working Group II to the Fifth Assessment Report of the Intergovernmental Panel on Climate Change*. United Kingdom and New York, NY, USA: Cambridge University Press, Cambridge, pp. 361-409.

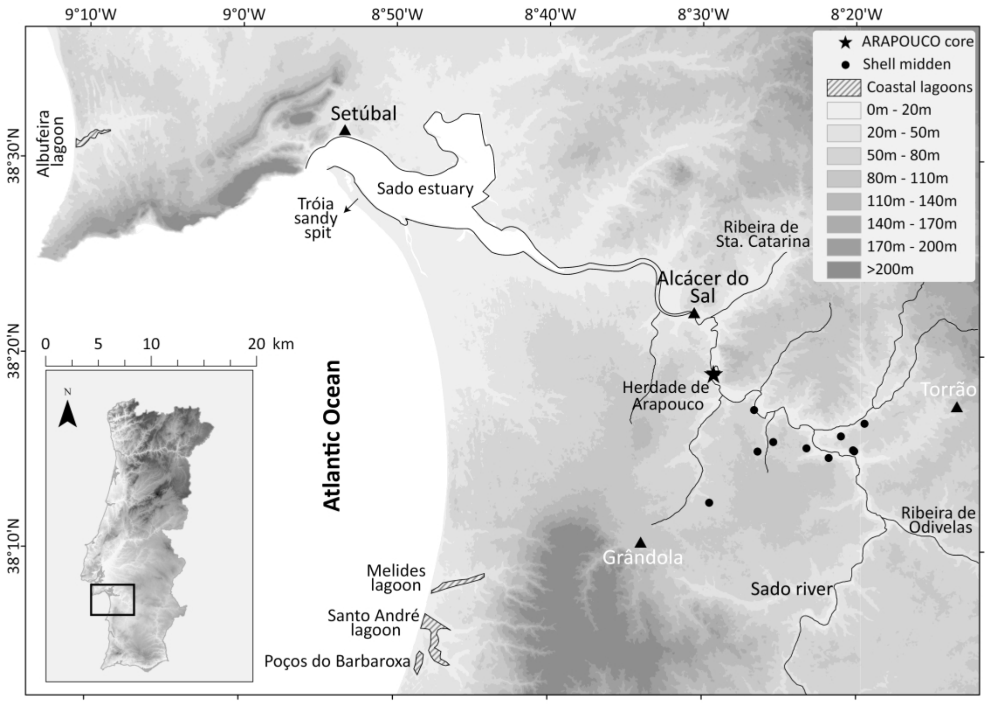

Figure 1 - Location of the Arapouco sediment core (black star).

420x298mm (300 x 300 DPI)

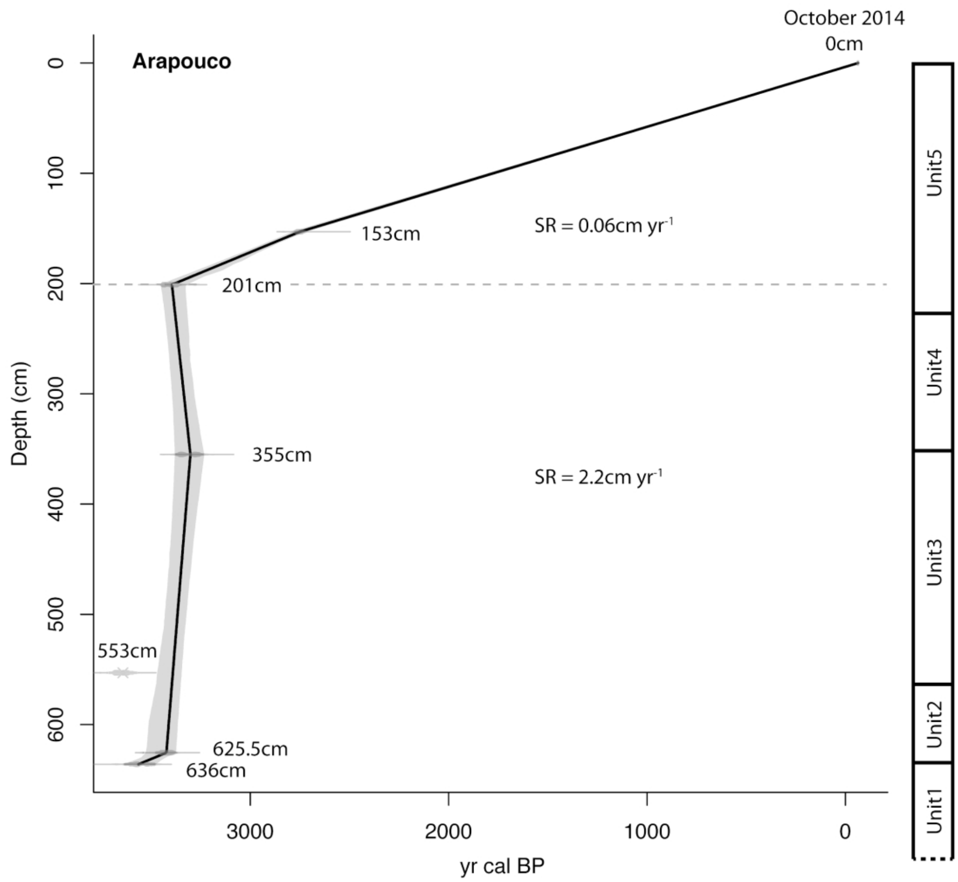

Figure 2 - 14C BP dates and age model with representation of the samples used for 14C dating done with Clam 2.2 software (Blaauw, 2010). and using the IntCal13 calibration curve (Reimer et al., 2013).

198x190mm (300 x 300 DPI)

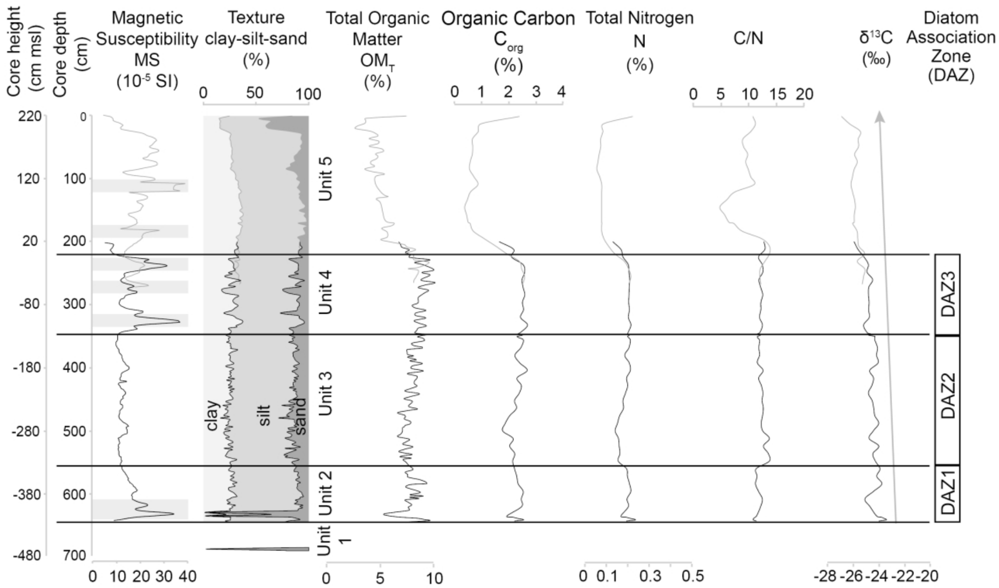

Figure 3 - Representation of sedimentological and organic proxies against depth below surface and height: magnetic susceptibility (MS), texture, total organic matter (OMT), organic carbon (Corg), total nitrogen (N), C/N and δ13C. The black line represents results obtained from Arapouco3 and the grey line results from Arapouco2 sections. Both present the same behaviour in the overlapping region. Grey bars in MS profile represent higher inputs of terrestrial material (see discussion below). The black arrow indicates the decreasing trend of δ13C upcore.

240x144mm (300 x 300 DPI)

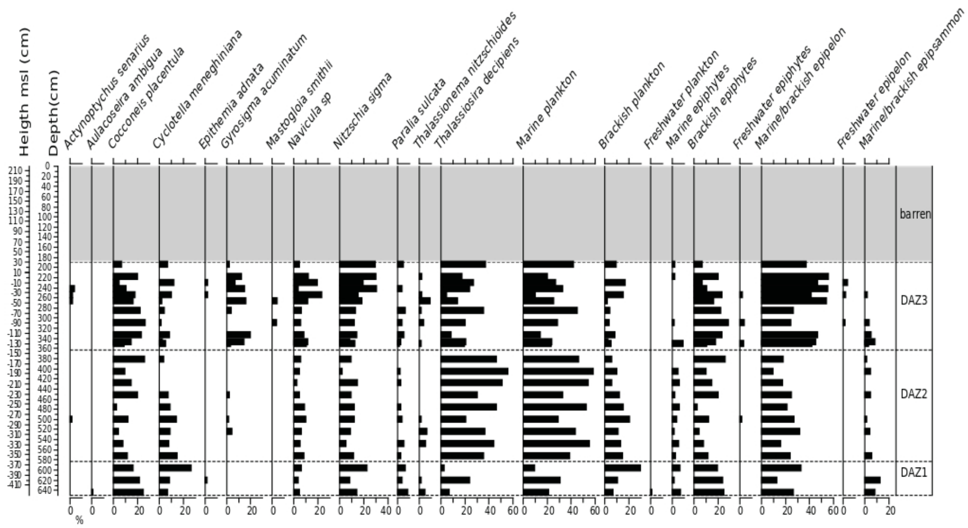

Figure 4 – Down-core distribution of selected diatom taxa and diatom-assemblages zones (DAZ) in the sediment record plotted against core depth and msl height.

372x287mm (72 x 72 DPI)

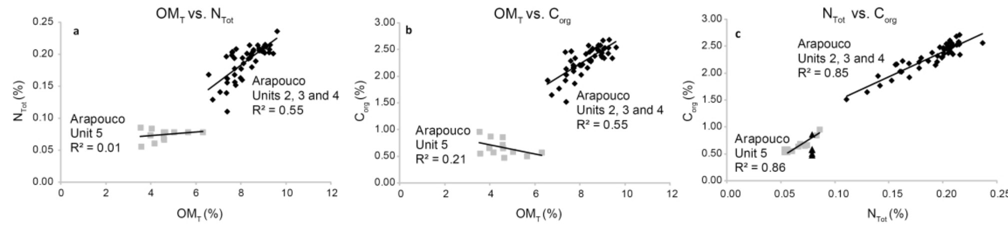

Figure 5 – Correlation between: a - OMT and NTot; b - OMT and Corg; c - NTot and Corg (c). Black diamonds represent samples from Units 2, 3 and 4 and grey squares represent samples from Unit 5. Black triangles (c) represent samples enriched in NTot.

396x87mm (300 x 300 DPI)

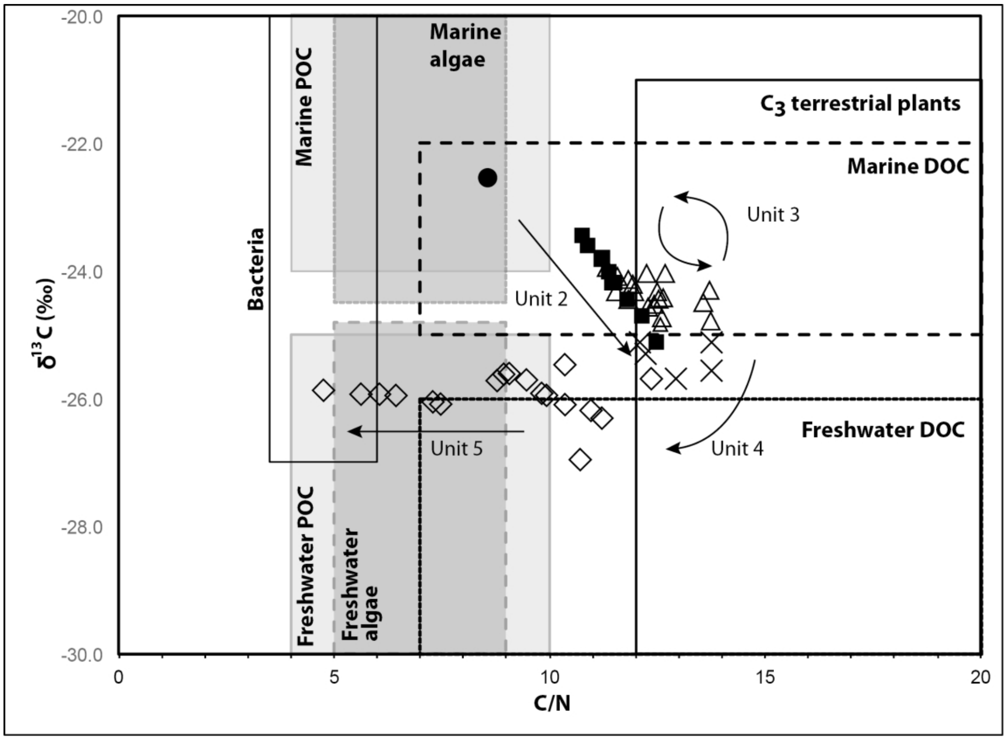

Figure 6 – C/N vs. δ13C results plotted at adapted Lamb et al.'s graph (2006). Black filled squares represent Unit 2; black triangles represent Unit 3; black crosses represent Unit 4, and black diamonds represent Unit 5. The black circle represents the sediment collected in the main channel at Arapouco in 2017.

200x146mm (300 x 300 DPI)

Core reference	**Easting**	**Northing**	**Elevation of ground surface at core location (m *msl*)**	**Start collection point (m *msl*)**	**End collection point (m *msl*)**	**Collected core length (cm)**
Arapouco2	-31026.1743	-149671.94	2.2	2.2	-0.48	268
Arapouco3	-31030.6767	-149673.241	2.2	0.2	-4.70	490

Sample reference	Lab code	Material	Core depth (cm)	$\delta^{13}C$ (‰)	Conventional ^{14}C age BP	Calibrated age BP (95%)
Arapouco2#9 152-154	Beta-436176	Organic sediment	153	-25.4	2620±30	2778-2726
Arapouco2#10 200-202	Beta-408535	Organic sediment	201	-25.4	3170±30	3452-3349
Arapouco3#2 354-356	Beta-393523	Organic sediment	355	-22.7	3100±30	3379-3235
Arapouco3#4 552-554	Beta-408534	Organic sediment	553	-23.5	3400±30	3711-3573
Arapouco3#5 624-627	Beta-431370	Organic sediment	625.5	-23.4	3210±30	3542-3368
Arapouco3#5 635-637	Beta-431371	Organic sediment	636	-23.5	3330±30	3636-3479